

# Entanglement Spectra of Quantum Heisenberg Ladders

Didier Poilblanc

Laboratoire de Physique Théorique UMR5152, CNRS and Université de Toulouse, F-31062 France  
(Received 19 May 2010; revised manuscript received 29 June 2010; published 13 August 2010)

Bipartite entanglement measures are surprisingly useful tools to investigate quantum phases of correlated electrons. Here, I analyze the entanglement spectrum of *gapped* two-leg quantum Heisenberg ladders on a periodic ribbon partitioned into two identical periodic chains. The entanglement spectrum closely reflects the low-energy gapless spectrum of each individual edge. This extends the conjecture initially drawn for fractional quantum Hall systems to the field of quantum magnetism, stating a direct correspondence between the low-energy entanglement spectrum of a partitioned system and the true spectrum of the *virtual edges*. A mapping of the reduced density matrix to a thermodynamic density matrix is also proposed via the introduction of an effective temperature.

DOI: 10.1103/PhysRevLett.105.077202

PACS numbers: 75.10.Jm, 05.30.Rt

**Introduction.**—The recent application of quantum information concepts to several domains of condensed matter [1] has proven to be extremely successful, giving new types of physical insights on exotic quantum phases. Upon partitioning a many-body quantum system into two parts  $A$  and  $B$ , quantum entanglement can be characterized by the properties of the ground state reduced density matrix of either one of the two parts,  $\rho_A$  or  $\rho_B$ . For example, entanglement entropies such as the von Neumann entropy  $-\text{Tr}\{\rho_A \ln \rho_A\}$  or the family of Rényi entropies offer an extraordinary tool to identify a one-dimensional conformal invariant system [2] and provide, e.g., a direct (numerical) calculation of its central charge [3].

Furthermore, the entanglement spectrum (ES) defined by the eigenvalues of a fictitious Hamiltonian  $\mathcal{H}$ , where  $\rho_A$  is written as  $\exp(-\mathcal{H})$ , has been shown to provide much more complete information on the system. In one dimension, underlying conformal field theory (CFT) leads to universal scalings of the ES (Ref. [4]), and topological properties of the ground state (GS) can be reflected by specific degeneracies [5]. By choosing a partition corresponding to a very nonlocal real-space cut, the ES has also been used to define nonlocal order in gapless spin chains [6].

Many-particle quantum entanglement is also a powerful tool to characterize topological features of a two-dimensional GS (Ref. [7]) as, e.g., in dimer liquids on a cylinder geometry [8]. Also, bipartite ES have been shown to provide valuable information on the edge states of fractional quantum Hall states on spherical [9] and torus geometries [10] upon partition into two (identical) subsystems. Interestingly, the ES of the incompressible GS of a generic Landau-level-projected Coulomb Hamiltonian arranges into a low-energy CFT spectrum separated by an “entanglement gap” from the high-energy levels, a fingerprint of topological order [9,11].

Such advanced insightful analysis of the ES has not, however, been fully exploited in low-dimensional quantum magnets. In particular, the conjecture by Haldane of a precise correspondence between the entanglement spec-

trum and the true spectrum in reduced space, e.g., the spectrum of the subsystem  $A$ , is of very high interest and so far supported only by limited calculations on quantum Hall systems. [9,10] Low-dimensional quantum magnets offer a completely different class of many-body systems where new aspects of this correspondence can be investigated, giving further insights on this fascinating scenario.

**Model and system.**—I consider here a two-leg ladder made of two quantum Heisenberg spin-1/2 chains coupled via a “rung” exchange coupling  $J_{\text{rung}}$ , as shown in Fig. 1(a). Such a quantum magnetic ladder [12] offers an attractive although still simple system with three nontrivial phases, as shown in the phase diagram in Fig. 1(b), depending on the signs of the leg (i.e., within the chains) and rung Heisenberg exchange couplings, parametrized as  $J_{\text{leg}} = \cos\theta$  and  $J_{\text{rung}} = \sin\theta$ , respectively. I shall not consider here the case when both couplings are ferromagnetic leading to a trivial fully polarized ferromagnet (lower-left quadrant). The physics of the other two phases (occupying the three remaining quadrants) can be easily understood by starting from the strong rung coupling limit, i.e., when  $|J_{\text{rung}}| \gg J_{\text{leg}}$ . When  $J_{\text{leg}} = 0$ , spin singlets or triplets

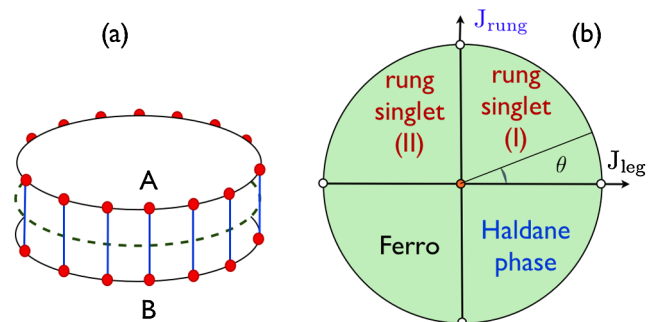


FIG. 1 (color online). (a) Ribbon made of two coupled periodic Heisenberg chains (two-leg ladder). The partition into two identical  $A$  and  $B$  subsystems is made by cutting the rungs along the dashed line. (b) Phase diagram of the two-leg ladder mapped onto a circle assuming  $J_{\text{leg}} = \cos\theta$  and  $J_{\text{rung}} = \sin\theta$ .

form on the rungs depending on whether the rung coupling is antiferromagnetic (AFM) or ferromagnetic (FM). For an AFM rung coupling  $J_{\text{rung}} > 0$ , upon turning on a leg coupling of either sign, the product of rung singlets smoothly evolves into a (gapped) “rung singlet” phase. For a FM rung coupling  $J_{\text{rung}} < 0$  and a small AFM leg coupling  $J_{\text{leg}} > 0$ , the ladder system can be mapped onto an effective gapped spin-1 chain [13] yielding an effective “Haldane phase” [14,15]. Remarkably, such gapped phases remain stable all the way to the weakly coupled chain regime. The rung coupling is therefore a “relevant” perturbation. For example, while the spectrum of the decoupled AFM chains system is the tensor product of two gapless CFT invariant spectra [16] of central charge  $c = 1$ , any finite  $J_{\text{rung}}$  opens a gap. Note also that the two rung singlet phases for AFM and FM leg couplings labeled as (I) and (II) in Fig. 1(b) are smoothly connected to each other. Extension to frustrated interchain couplings is also considered [17].

The finite size two-leg ladder of Fig. 1(a) is topologically equivalent to a ribbon which can be partitioned into two halves  $A$  and  $B$  preserving periodic boundary conditions. This offers a simple convenient setup to investigate the entanglement between the two chain subsystems as a function of their coupling  $J_{\text{rung}}$ . I report below the entanglement entropies as well as entanglement spectra in the two considered gapped phases, computed numerically on  $2 \times 10, 2 \times 12$ , and  $2 \times 14$  clusters. It is shown that the ES reflects the underlying CFT scaling behavior of the isolated chains. This is remarkable, in particular, in the strong rung coupling limit where the two subsystems are strongly entangled producing a short spin correlation length. Note that I am considering here a different setup than the one used by Kallin *et al.* [18] to calculate entanglement entropies on  $N$ -leg Heisenberg ladders.

**Results.**—Characterizing the entanglement between  $A$  and  $B$  requires the knowledge of the reduced density matrix  $\rho_A$  of the  $A$  subsystem. After computing the GS by Lanczos exact diagonalization on finite  $2 \times L$  periodic clusters, an explicit use of translation symmetry enables one to express  $\rho_A$  in a block-diagonal form, where each block corresponds to an irreducible representation labeled by one of the (allowed) total momentum  $K = 2\pi \frac{p}{L}$ ,  $p = -L/2 + 1, \dots, L/2$ . These blocks can then be diagonalized (separately) to compute the von Neumann (VN) entropy  $S_{\text{VN}} = -\text{Tr}\{\rho_A \ln \rho_A\}$  or the family of Rényi entropies [19]  $S_n = \frac{1}{1-n} \ln \text{Tr}\{(\rho_A)^n\}$ ,  $n \geq 2$ . Note that  $S_{\text{VN}}$  can be considered as  $\lim_{n \rightarrow 1} S_n \equiv S_1$ . Results for  $S_{\text{VN}}$  and  $S_2$  in the Haldane and rung singlet phases (for  $J_{\text{leg}} > 0$ ) are reported in Fig. 2. The single-copy entanglement [20] obtained by taking the limit  $n \rightarrow \infty$  and given by  $S_\infty = -\ln \lambda_0$ , where  $\lambda_0$  is the largest eigenvalue of  $\rho_A$ , is also shown for comparison [21]. An inspection of the finite size scaling of the data reveals that the leading term of all entanglement entropies is proportional to the size  $L$  (corresponding to the length of the edge between  $A$  and  $B$ ) as expected from the area law. The data are therefore normal-

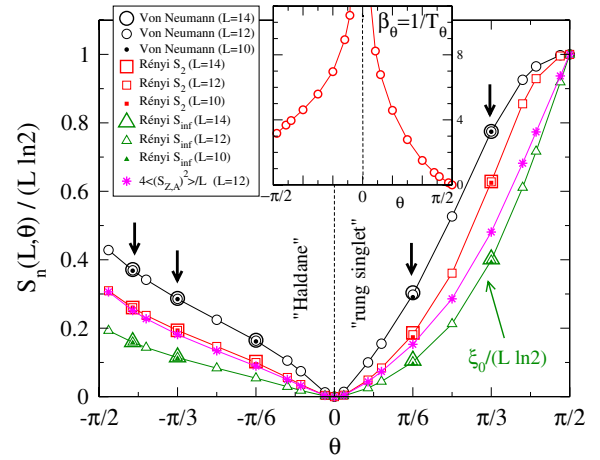


FIG. 2 (color online). Various  $S_n$  entanglement entropies ( $n = 1$  von Neumann  $S_{\text{VN}}$  entropy;  $n = 2$  and  $n = \infty$  Rényi entropies) computed on  $2 \times L$  ladders of length up to  $L = 14$ , normalized by  $L \ln 2$  and plotted versus the angle  $\theta$ . Note that  $\xi_0 = S_\infty \equiv S_{\text{inf}}$ . Only the two right quadrants of Fig. 1(b) are considered. For comparison, the fluctuation of  $S_A$  (normalized by  $3L/4$ ) is also plotted (stars). The corresponding ES are shown in Fig. 3 for the values of  $\theta$  marked by arrows. Inset: Effective inverse temperature  $\beta_\theta$  (see text).

ized by  $L \ln 2$ , which is the maximum entanglement entropy obtained for the product of independent rung singlets ( $\theta = \pi/2$ ). The finite size corrections (details in supplementary material [17]) are found to be very small. As also expected, all  $S_n$  vanish in the limit of decoupled chains, where the GS becomes a simple product state. Interestingly, the behaviors of  $S_{\text{VN}}$  and  $S_2$  are fairly similar, showing the same linear (quadratic) behavior with  $J_{\text{leg}} \sim \Delta\theta$  in the strong rung coupling limit  $\theta \rightarrow -\pi/2$  ( $\theta \rightarrow \pi/2$ ). In contrast to  $S_{\text{VN}}$  and  $S_2$ ,  $S_\infty$  behaves linearly when  $\theta \rightarrow \pi/2$ , a behavior also seen in the quantum fluctuation of the total spin  $S_A$  of the  $A$  subsystem [22].

I now move to the ES, which contains more information, defined as the spectrum  $\{\xi_\alpha\}$  of the Hermitian operator  $\mathcal{H}$  given by the relation  $\rho_A = \exp(-\mathcal{H})$ . The  $\xi_\alpha$  can then be obtained from the weights  $\lambda_\alpha$  of  $\rho_A$  as  $\xi_\alpha = -\ln \lambda_\alpha$ . Typical ES (measured from the GS energy  $\xi_0$ ) plotted as a function of momentum  $K$ , for the three sizes, are shown in Fig. 3, both in the rung singlet [(a) and (b)] and the Haldane [(c) and (d)] phases. Note that the total spin  $S_A = S$  is also a good quantum number which can be assigned to each level. It is remarkable that the low-energy excitations are spin-triplet that accurately resemble the des Cloiseaux-Pearson spectrum [23] of the quantum Heisenberg chain (up to a multiplicative factor); in particular, two gapless modes at  $K = 0$  and  $K = \pi$  [24] are clearly visible. The lowest singlet excitations close to  $K = 0$  and  $K = \pi$  also form towers of states as predicted for the Heisenberg chain [25]. This suggests strongly that the ES bears the *same* low-energy CFT structure. In that case, we expect, in particular, the GS energy  $\xi_0$  to scale as

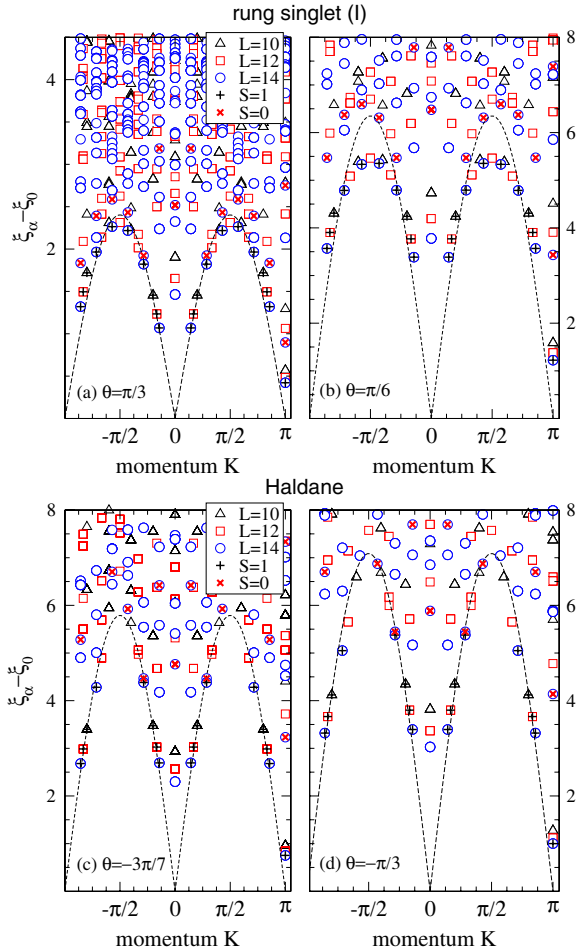


FIG. 3 (color online). Entanglement excitation spectra versus total momenta  $K$  in the chain direction for four different values of  $\theta$  (shown by arrows in Fig. 2) corresponding to the rung singlet (I) phase (a),(b) and the Haldane phase (c),(d). All low-energy excitations computed on  $2 \times 10$ ,  $2 \times 12$ , and  $2 \times 14$  ladders are shown by open (black) triangles, (red) squares, and (blue) circles, respectively. The lowest triplet eigenstates (for all  $L$ ) are marked by (black) + symbols and are fitted as  $\Delta\xi = v|\sin(K)|$  by dashed lines. The lowest singlet eigenstates for  $L = 14$  are also marked by (red)  $\times$  symbols.

$$\xi_0/L = e_0 + d_1/L^2 + \mathcal{O}(1/L^3). \quad (1)$$

Such a behavior is indeed found for strong AFM rung couplings where  $L \gg l_{\text{mag}}$ . Furthermore, the fit provides a number in good agreement with the CFT prediction  $d_1 = \pi cv/6$ , where  $v$  is the velocity of the triplet mode of the ES and the central charge  $c$  is set to 1. For example, for  $\theta = \pi/3$ , the fit gives  $d_1 \approx 1.31$ , which compares well to  $\pi cv/6 \approx 1.24$  estimated from the data of Fig. 3(a). Note that for smaller rung couplings at which  $L \sim l_{\text{mag}}$  this scaling law is no longer satisfied [17].

I finish the investigation of entanglement spectra by considering the rung singlet (II) phase realized for a ferromagnetic leg coupling ( $J_{\text{leg}} < 0$ ) and an AFM rung coupling  $J_{\text{rung}} > 0$  [upper left quadrant of the phase diagram in Fig. 1(b)] and smoothly connected to the limit of de-

coupled rung singlets ( $\theta = \pi/2$ ,  $J_{\text{leg}} = 0$ ). The results of the ES of  $2 \times 10$  and  $2 \times 14$  ladders are shown in Figs. 4(a) and 4(b) for strong and weak rung couplings, respectively. At low energies, the ES are shown to coincide (up to an overall factor) with the spectrum of the ferromagnetic quantum Heisenberg chain, consisting of  $m$ -magnon bound states (or solitons) [26] given by  $E_m(K) = 2J_{\text{eff}}\sin^2(K/2)/m$ , where  $J_{\text{eff}}$  is an effective chain coupling. On a finite cluster, such multimagnon excitations are subject to the kinematic constraint  $K \geq 2\pi m/L$ , where  $L$  is the ladder length. Therefore, the lower-bound energy “envelope” behaves as  $E_{\text{min}}(K) \sim \frac{4\pi}{L}J_{\text{eff}}\sin^2(K/2)/K$  up to small finite size corrections, as shown in Fig. 4 [note  $E_{\text{min}}(K) \rightarrow 0$  for all  $K$  in the thermodynamic limit].

All these results on quantum ladders support the conjecture of a deep correspondence between the ES and the true spectrum of the (virtual) edges.

*Effective temperature.*—Finally, I suggest that the density matrix  $\rho_A$  can be rewritten as a thermodynamic density matrix by simply introducing an effective, model-parameter-dependent, temperature scale  $T_\theta$  (focusing on the  $J_{\text{leg}} > 0$  case). Indeed, comparison of Figs. 3(a) and 3(b), on one hand, and of Figs. 3(c) and 3(d), on the other hand, reveals almost identical spectra after rescaling. This implies that  $\rho_A$  can be written as

$$\rho_A = \frac{1}{z_\theta} \exp(-\beta_\theta \hat{h}), \quad (2)$$

where  $\hat{h}$  is a parameter-free (extensive) Hamiltonian,  $z_\theta = \lambda_0^{-1}$ , and  $\beta_\theta = T_\theta^{-1}$ . Since, as shown in Fig. 3, the spectrum of  $\hat{h}$  has the same  $c = 1$  low-energy CFT structure as

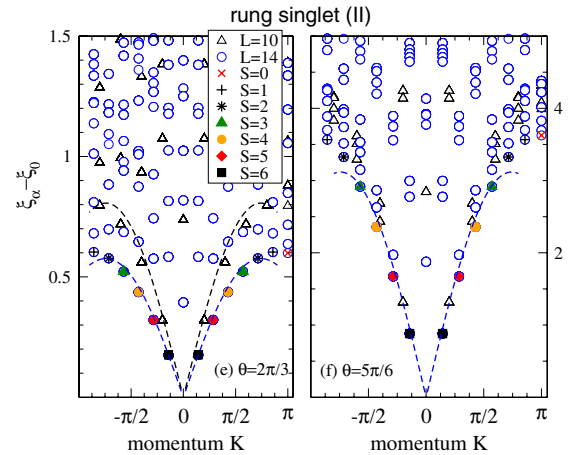


FIG. 4 (color online). (e),(f) The same as Fig. 3 for the rung singlet (II) phase (only  $L = 10$  and  $L = 14$  are shown). Here the GS is the saturated ferromagnet. The total spins  $S$  of the lowest eigenstates are indicated by different symbols (and colors) and can be assigned to  $m$ -magnon bound states,  $m = S_{\text{max}} - S = L/2 - S$ . The lowest-energy excitations for  $L = 14$  are fitted according to  $E_{\text{min}}(K)$  (see text). In (e), the fit for  $L = 14$  rescaled by a factor  $14/10$  (upper dotted line) also gives good agreement with the  $L = 10$  data.

the Heisenberg chain Hamiltonian,  $\hat{h}$  can be “normalized” by, e.g., fixing the velocity  $v$  of the triplet branch to be  $v_{\text{Heis}} = \pi/2$ , the Heisenberg chain value. The effective inverse temperature  $\beta_\theta$  is simply adjusted to the actual slope of the gapless ( $K = 0$ ) mode of the corresponding ES and is reported in the inset in Fig. 2 as a function of  $\theta$ . Apart from logarithmic corrections, the thermal (magnetic) length is  $l_{\text{1D}} \sim T_\theta^{-1}$  (Ref. [27]), which, heuristically, can be associated (up to a prefactor of order 1) to the ladder correlation length  $l_{\text{mag}}$ . Therefore, the behavior of  $\beta_\theta$  in the inset in Fig. 2 simply reflects the behavior of  $l_{\text{mag}}$  with  $\theta$ . In particular, in the strong AFM rung coupling regime  $J_{\text{rung}} \gg J_{\text{leg}}$ ,  $\beta_\theta$  is linear in  $\theta - \pi/2$ , in agreement with the numerical estimation of  $l_{\text{mag}}$ ,  $l_{\text{mag}} \propto J_{\text{leg}}$ . More generally, within our normalization of  $\hat{h}$ ,  $\beta_\theta \sim l_{\text{mag}}/2$ . Also, it is interesting here to use the exact equivalence between the entanglement VN entropy and the thermodynamic entropy of the (effective) finite- $T$  subsystem. In the regime of weakly coupled chains, using the expression of the thermodynamic entropy of the Heisenberg AFM chain when  $T_\theta \ll 1$ , one predicts  $S_{\text{VN}}/L \sim \pi T_\theta/(3v_{\text{Heis}})$  (assuming again  $c = 1$ ), which agrees (within less than 15% difference) with the calculated VN entropy, giving further support that  $\hat{h}$  belongs to the same universality class as the AFM Heisenberg chain (for  $J_{\text{leg}} > 0$ ).

*Concluding remarks.*—In this Letter, I showed that the ES of the (ground state) reduced density matrix of a two-leg quantum ladder possesses remarkable universal features one can associate to its two single Heisenberg chain subsystems. This strongly supports a broader applicability (beyond quantum Hall systems) of the conjecture by Haldane establishing a deep correspondence between the ground state ES of a many-body system made of two entangled constituents with the true spectra of the virtual edges. For example, although for AFM leg coupling the two ground states of the quantum ladder at  $\theta > 0$  and  $\theta < 0$  belong to distinct topological sectors of the singlet spin Hilbert space [15] characterized by different “string orders,” it is remarkable that a similar  $c = 1$  CFT low-energy ES is found and that Eq. (2) applies to both cases. Similarly, although the two rung singlet phases (I) and (II) are smoothly connected, they exhibit completely different low-energy ES in straight connection to the different nature of their edges. Last, I notice that the results of this Letter also apply to the case of frustrated ladders [17].

I am indebted to S. Capponi, N. Laflorencie, G. Misguich, M. Haque, and P. Pujol for interesting suggestions and/or comments. I thank IDRIS (Orsay, France) for allocation of CPU time on the NEC-SX8 supercomputer.

[1] L. Amico, R. Fazio, A. Osterloh, and V. Vedral, *Rev. Mod. Phys.* **80**, 517 (2008).

[2] John Cardy and Pasquale Calabrese, *J. Phys. A* **42**, 504005 (2009), and references therein.

- [3] M. Fühlinger, S. Rachel, R. Thomale, M. Greiter, and P. Schmitteckert, *Ann. Phys. (Berlin)* **17**, 922 (2008).
- [4] P. Calabrese and A. Lefevre, *Phys. Rev. A* **78**, 032329 (2008).
- [5] Franck Pollmann, Ari M. Turner, Erez Berg, and Masaki Oshikawa, *Phys. Rev. B* **81**, 064439 (2010).
- [6] Ronny Thomale, D.P. Arovas, and B. Andrei Bernevig, *arXiv:0912.0028* [Phys. Rev. Lett. (to be published)].
- [7] A. Kitaev and J. Preskill, *Phys. Rev. Lett.* **96**, 110404 (2006); M. Levin and X.G. Wen, *Phys. Rev. Lett.* **96**, 110405 (2006).
- [8] J.-M. Stéphan, S. Furukawa, G. Misguich, and V. Pasquier, *Phys. Rev. B* **80**, 184421 (2009).
- [9] Hui Li and F.D.M. Haldane, *Phys. Rev. Lett.* **101**, 010504 (2008).
- [10] N. Regnault, B. A. Bernevig, and F.D.M. Haldane, *Phys. Rev. Lett.* **103**, 016801 (2009); A.M. Läuchli, E.J. Bergholtz, J. Suorsa, and M. Haque, *Phys. Rev. Lett.* **104**, 156404 (2010).
- [11] R. Thomale, A. Sterdyniak, N. Regnault, and B. A. Bernevig, *Phys. Rev. Lett.* **104**, 180502 (2010).
- [12] E. Dagotto and T.M. Rice, *Science* **271**, 618 (1996); numerical simulations can be found in T. Barnes, E. Dagotto, J. Riera, and E.S. Swanson, *Phys. Rev. B* **47**, 3196 (1993); M. Troyer, H. Tsunetsugu, and D. Würtz, *Phys. Rev. B* **50**, 13515 (1994); M. Greven, R.J. Birgeneau, and U.-J. Wiese, *Phys. Rev. Lett.* **77**, 1865 (1996).
- [13] In the limit of vanishing  $J_{\text{leg}}$ , the spin gap equals  $\sim 0.41 \times 2J_{\text{leg}}$  and the spin correlation length is  $l_{\text{mag}} \sim 6.01$ .
- [14] F.D.M. Haldane, *Phys. Rev. Lett.* **50**, 1153 (1983); for numerical simulations, see S. Todo and K. Kato, *Phys. Rev. Lett.* **87**, 047203 (2001).
- [15] For topological properties, see E.H. Kim, G. Fáth, J. Sólyom, and D.J. Scalapino, *Phys. Rev. B* **62**, 14965 (2000); F. Anfuso and A. Rosch, *Phys. Rev. B* **75**, 144420 (2007).
- [16] The Heisenberg spin-1/2 chain belongs to the  $SU(2)_1$  Wess Zumino Witten universality class.
- [17] See supplementary material at <http://link.aps.org/supplemental/10.1103/PhysRevLett.105.077202> for frustrated interchain couplings.
- [18] A.B. Kallin, I. Gonzalez, M.B. Hastings, and R.G. Melko, *Phys. Rev. Lett.* **103**, 117203 (2009).
- [19]  $S_2$  can also be computed with quantum Monte Carlo calculations in *nonfrustrated* AFM Heisenberg magnets. See M.B. Hastings, I. Gonzalez, A.B. Kallin, and R.G. Melko, *Phys. Rev. Lett.* **104**, 157201 (2010).
- [20] For  $S_\infty$  in critical spin chains, see, e.g., J. Eisert and M. Cramer, *Phys. Rev. A* **72**, 042112 (2005).
- [21] Recall that  $S_{\text{VN}} \equiv S_1 \geq S_2 \geq \dots \geq S_\infty$ .
- [22] H. Francis Song, Stephan Rachel, and Karyn Le Hur, *Phys. Rev. B* **82**, 012405 (2010).
- [23] J. des Cloiseaux and J.J. Pearson, *Phys. Rev.* **128**, 2131 (1962).
- [24] For  $L = 4p + 2$ ,  $K$  is shifted as  $K \rightarrow K - \pi$ .
- [25] F. Woynarovich, *Phys. Rev. Lett.* **59**, 259 (1987).
- [26] H. A. Bethe, *Z. Phys.* **71**, 205 (1931); H. C. Fodgedby, *J. Phys. C* **13**, L195 (1980); F.D.M. Haldane, *J. Phys. C* **15**, L1309 (1982).
- [27] K. Nomura and M. Yamada, *Phys. Rev. B* **43**, 8217 (1991).